JOURNAL OF SPACECRAFT AND ROCKETS
Vol. 43, No. 5, September–October 2006

Micromechanical Models for Bending Behavior of Woven Composites

Ömer Soykasap*
Afyon Kocatepe University, 03200 Afyonkarahisar, Turkey

DOI: 10.2514/1.18010

Thin woven composites have been popular for space structures due to the symmetrical and balanced properties. Although in-plane properties of these materials can be estimated accurately using the classical lamination theory, the corresponding bending properties lack any accuracy for one- or two-ply woven laminates. Such estimates can result in errors of up to 200% in the maximum bending strains or stresses, and up to 400% in the bending stiffnesses. This paper presents micromechanical models for bending behavior of woven composites considering the fiber bundles and the matrix and their interactions. First, homogenized material properties are predicted by a mosaic model based on the classical lamination theory. Then, higher fidelity finite element models are developed to estimate the bending properties of plain-weave composites. The results of finite element model are compared with experimental data, showing good agreement, particularly for a lamina.

I. Introduction

THIN woven composites have been popular for space structures due to the symmetrical and balanced properties coupled with very good handling and damage characteristics. Their use in ultrathin deployable structures is of current interest, where it is envisaged that a laminate will consist of only a small number of plies. Woven composites have different styles, such as plain weave, twill, and satin. Material properties depend on the number of fibers in warp and weft directions as well as the type of weave. The type of the weave is also important because it determines processability of the composite, such as drapeability over a curved surface. In plain-weave style, each warp fiber passes alternately over and under each fill (weft) fiber (see Fig. 1). This paper studies bending behavior of plain-weave composites.

A schematic cross section of a plain-weave lamina is shown in Fig. 2, where h and L are the amplitude of the wave formed by the centerline of the fibers and their wave length. Images of the cross section of plain-weave laminate, obtained with an optical microscope, are shown in Fig. 3.

The estimation of the mechanical properties of these thin laminates is crucial for the design of future deployable structures. There have been many micromechanical homogenization schemes to determine in-plane properties of woven laminates analytically. For example, Naik [1] presents a unit-cell model to predict overall, three-dimensional, thermal, and mechanical properties of woven composites. Johnson et al. [2] study the effect of crimp angles, yarn size, and matrix properties on the average elastic moduli of woven materials. On the other hand, detailed finite element (FE) models have been developed to estimate the material properties of woven composites more accurately. For example, Fujita et al. [3] and Dano et al. [4] used beam elements to study in-plane properties of woven composites, recently Bednarcyk and Arnold [5] developed three-dimensional repeating unit-cell model to study woven composites, and more recently Le Page et al. [6] developed two-dimensional FE model to study damage properties.

Although the in-plane properties of a thin laminate can be calculated with good accuracy using classical lamination theory (CLT), the bending properties of these materials lack any accuracy for one or two-ply woven laminates. Experiments on thin laminates made from woven composites disagree with the predictions of the bending stiffnesses and strains using CLT [7]. The bending properties obtained from CLT can result in errors of up to 200% in the maximum bending strains or stresses, and up to 400% in the bending stiffnesses. The problem is that CLT assumes that the fibers and the matrix are uniformly distributed in each lamina, uses in-plane material properties to analyze the macromechanical behavior of a laminate, and relies on this uniformity in the integration of the transformed laminate stiffnesses over the thickness of the laminate [8]. However, it is clear from Fig. 3 that a thin laminate made from fabrics in fact consists of bundles of fibers (called yarn) that are typically much thinner than the overall thickness of the laminate; these bundles are not homogenous through the thickness and hence CLT needs to be used with great care in the present case.

This paper presents micromechanical models for bending behavior of woven composites considering the fiber bundles, the matrix, and their interactions. First homogenized material properties are predicted by a mosaic model using CLT. Then higher fidelity finite element models are developed to predict the bending properties of plain-weave T300/LTM45 composite. Initially curved beam elements are used to model each infiltrated fiber bundle. Interlaced bundles are constrained at the crossover points, representing the resin interface. A geometrically nonlinear analysis of the resulting "space frame" is carried out to investigate the behavior of one-, two-, and three-ply woven composites.

II. Material Properties

In the present study, T300/LTM45 plain-weave composite manufactured by Brookhouse Paxford, U.K., is studied. Plain-weave T300 is made of 1000 fibers, and has an areal weight of 94 g/m^2. LTM45 matrix cures at a temperature of 60°C for 9 h. Material properties of the fiber and the matrix are given in Table 1.

Homogenized material properties of each infiltrated yarn are based on the properties of the fibers and the matrix, and their contributions. Based on measurements from micrographs, T300/LTM45 plain-weave lamina has the amplitude of the wave formed by the centerline of the fibers, $h = 0.0275$ mm, and the wavelength of $L = 2.75$ mm (see Fig. 2). The thickness of each infiltrated yarn is taken to be half of the thickness of the composite $t = 0.11$ mm. The cross section of the yarn is approximated as a rectangle 1.375×0.055 mm, taking the equivalent area of a lenticular-shaped yarn. T300 filament has a diameter of 6.9 μm, and the total cross-sectional area of 1000 fibers

Presented as Paper 2264 at the the 46th AIAA/ASME/ASCE/AHS/ASC Structures, Structural Dynamics and Materials Conference, Austin, TX, 18–21 April 2005; received 3 June 2005; revision received 21 March 2006; accepted for publication 31 May 2006.

*Assistant Professor, Department of Mechanics. Member AIAA.

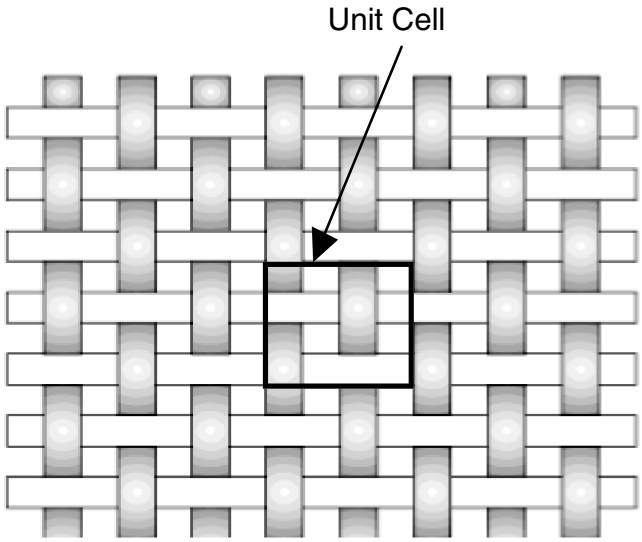

Fig. 1 Plain-weave style.

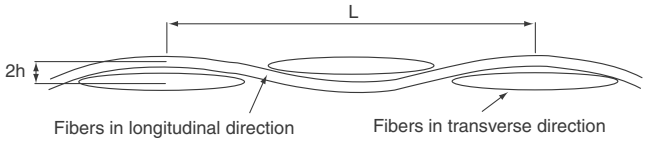

Fig. 2 Basic definitions of woven fiber microstructure.

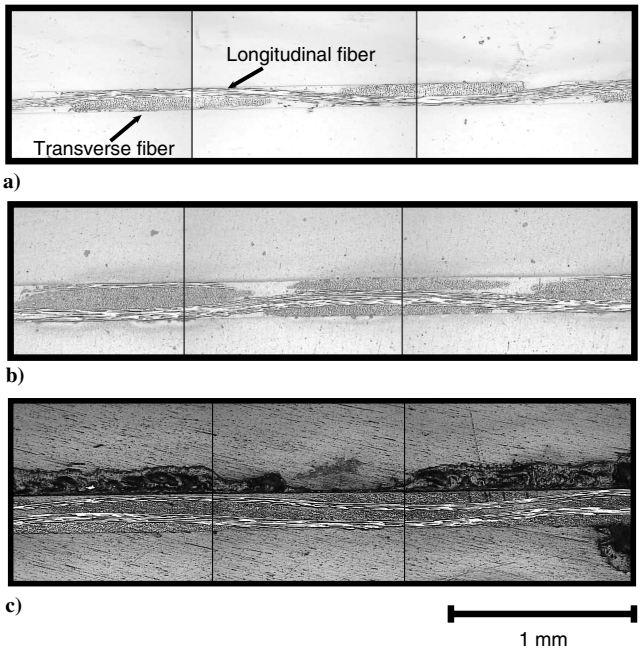

Fig. 3 Microstructure of LTM45; a) one ply, b) two plies (fibers out of phase), and c) two plies (fibers in phase).

is $A_f = 3.75 \times 10^{-2}$ mm^2, and hence fiber volume fraction V_f in the infiltrated yarn is then calculated as follows:

$$V_f = \frac{A_f}{A_y} = 0.5 \tag{1}$$

where $A_y = 1.375 \times 0.055$ mm^2 is the cross-sectional area of the yarn. Using the material properties given in Table 1 the homogenized material properties of a unidirectional yarn are obtained in what

Table 1 Material properties of T300 and LTM45

Property	T-300	LTM45
E_1, GPa	230	3.1
E_2, GPa	14	3.1
G_{12}, GPa	9	1.1
ν_{12}, GPa	0.2	0.41
Density, kg/m^3	1760	1230
Tensile strength, MPa	3530	——
Ultimate strain, %	1.5	——

follows. The longitudinal modulus of the yarn is obtained from the rule of mixtures

$$E_1^y = V_f E_{1f} + E_m(1 - V_f) = 116.6 \text{ GPa} \tag{2}$$

where E_{1f} and E_m are the elastic modulus of the fiber and the matrix, respectively. Although the rule of mixtures predicts the longitudinal modulus pretty well, the rule is not suitable for the prediction of transverse modulus. The transverse modulus and the shear modulus are obtained from the Halpin–Tsai equations [8] as follows:

$$E_2^y = \frac{(1 + \xi\eta V_f)E_m}{1 - \eta V_f} \tag{3}$$

where

$$\eta = \frac{E_{2f}/E_m - 1}{E_{2f}/E_m + \xi}$$

η is a measure of fiber reinforcement and depends on fiber geometry, packing geometry, and loading conditions. The value $\eta = 2$ is recommended for the fibers with circular cross section. This gives $E_2^y = 6.5$ GPa. The shear modulus is obtained with the reinforcing measure of $\eta = 1$ as follows:

$$G_{12}^y = G_m \frac{(G_{12f} + G_m) + V_f(G_{12f} - G_m)}{(G_{12f} + G_m) - V_f(G_{12f} - G_m)} = 2.5 \text{ GPa} \tag{4}$$

Major Poisson's ratio of the yarn is obtained from the fiber volume fraction and Poisson's ratios of the fiber and the matrix.

$$\nu_{12}^y = V_f \nu_{12f} + \nu_m(1 - V_f) = 0.305 \tag{5}$$

And the minor Poisson's ratio of the yarn is based on the reciprocity relationship

$$\nu_{21}^y = \nu_{12}^y \frac{E_2^y}{E_1^y} = 0.017 \tag{6}$$

A simple estimate of the homogenized elastic modulus and the Poisson's ratio of the woven lamina can be calculated using the rule of mixtures as follows:

$$E_1 = E_2 = 0.5 V_f E_{1f} + V_m E_m \tag{7}$$

$$\nu_{12} = \nu_{21} = 0.5 V_f \nu_{12f} + V_m \nu_m \tag{8}$$

where the coefficients of 0.5 in the first term on the right hand side is due to the fact that half of the fibers are in transverse direction.

III. Micromechanical Models

A. Properties of a Woven Laminate using CLT

Properties of a woven laminate are predicted using CLT, well-known equations of which are given next. According to CLT the constitutive equations for a thin plate (see Fig. 4) in terms of stress and strain resultants are

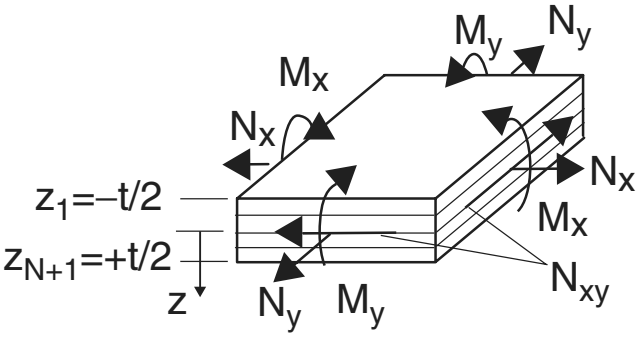

Fig. 4 Lay-up definition of a laminate.

$$\begin{Bmatrix} N \\ \cdots \\ M \end{Bmatrix} = \begin{bmatrix} A & \vdots & B \\ \cdots & & \cdots \\ B & \vdots & D \end{bmatrix} \begin{Bmatrix} \varepsilon^0 \\ \cdots \\ \kappa \end{Bmatrix} \tag{9}$$

where N is force resultants, M moment resultants, A extensional stiffness, B in-plane/flexure coupling stiffness, D bending stiffness, ε^0 midplane strains, and κ midplane curvatures. A, B, and D stiffnesses are defined in terms of the lamina stiffness $\bar{Q}_{ij}^k$ as

$$(A_{ij}, B_{ij}, D_{ij}) = \sum_{k=1}^{N} \int_{z_k}^{z_{k+1}} \bar{Q}_{ij}^k (1, z, z^2)\, \mathrm{d}z \tag{10}$$

or

$$A_{ij} = \sum_{k=1}^{N} \bar{Q}_{ij}^k (z_{k+1} - z_k) \tag{11}$$

$$B_{ij} = \frac{1}{2} \sum_{k=1}^{N} \bar{Q}_{ij}^k (z_{k+1}^2 - z_k^2) \tag{12}$$

$$D_{ij} = \frac{1}{3} \sum_{k=1}^{N} \bar{Q}_{ij}^k (z_{k+1}^3 - z_k^3) \tag{13}$$

The strains at any point in the laminate are calculated using midplane strains and the curvatures as follows:

$$\begin{bmatrix} \varepsilon_x \\ \varepsilon_y \\ \varepsilon_{xy} \end{bmatrix} = \begin{bmatrix} \varepsilon_x^o \\ \varepsilon_y^o \\ \varepsilon_{xy}^o \end{bmatrix} + z \begin{bmatrix} \kappa_x \\ \kappa_y \\ \kappa_{xy} \end{bmatrix} \tag{14}$$

If the laminate is symmetric $B_{ij} = 0$ and subject to only longitudinal curvature κ_x, corresponding bending moment and strain become

$$M_x = D_{11}\kappa_x \qquad \varepsilon_x = z\kappa_x \tag{15}$$

The maximum strain criterion assumes that failure occurs when the in-plane strains along the principal material direction exceed the ultimate strains of the material. When a unidirectional laminated plate is bent along its principal material direction, the maximum strain occurs on the outer edges of the plates, hence at $z = t/2$. Therefore, the minimum radius of curvature can be obtained from the ultimate strain $\varepsilon_{\max}$:

$$R_{\min} = \frac{t}{2\varepsilon_{\max}} \tag{16}$$

1. Single Ply

In CLT it is assumed that each layer is orthotropic with respect to its material symmetry, and is homogenous through the thickness. The simplistic approach is to use in-plane properties to calculate the lamina stiffness $\bar{Q}_{ij}^k$. However this would violate the assumption that the ply is homogenous through the thickness which it is clearly not. Therefore the simplistic approach would result in significant errors in the bending stiffnesses and hence in the bending strains and stresses. Homogenization through the thickness is performed by considering a repeating unit cell as shown in Fig. 1. First the unit cell is divided into subcells occupied by infiltrated yarns. The material properties of the subcell are based on the homogenized infiltrated yarn properties [5]. For the woven composite studied in this paper, there is no gap between warp and weft yarns; therefore the unit cell is represented by 4×4 mosaic model as seen in Fig. 5. The mosaic model consists of asymmetrical cross-ply laminates, and ignores the continuity and undulation of the fibers. Based on the isostrain assumption that the strains are spatially uniform, A, B, and D stiffnesses are then calculated considering the contributions of 0, 90, 0, 90 deg subcells over period L as follows:

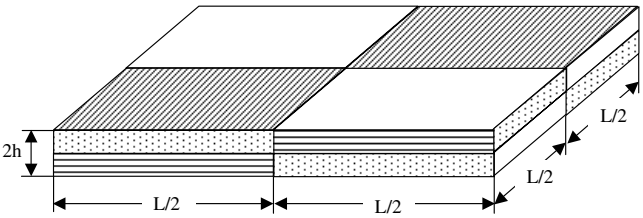

Fig. 5 4 × 4 mosaic model.

$$A_{ij} = \frac{1}{2}(hQ_{ij}^0 + hQ_{ij}^{90} + hQ_{ij}^{90} + hQ_{ij}^0) = h(Q_{ij}^0 + Q_{ij}^{90}) \tag{17}$$

$$B_{ij} = \frac{1}{2}\left(\frac{h^2}{2}Q_{ij}^0 - \frac{h^2}{2}Q_{ij}^{90} - \frac{h^2}{2}Q_{ij}^0 + \frac{h^2}{2}Q_{ij}^{90}\right) = 0 \tag{18}$$

$$D_{ij} = \frac{1}{2}\left(\frac{h^3}{3}Q_{ij}^0 + \frac{h^3}{3}Q_{ij}^{90} + \frac{h^3}{3}Q_{ij}^0 + \frac{h^3}{3}Q_{ij}^{90}\right) = \frac{h^3}{3}(Q_{ij}^0 + Q_{ij}^{90}) \tag{19}$$

where

$$Q_{11}^0 = Q_{22}^{90} = \frac{E_1^y}{1 - \nu_{12}^y \nu_{21}^y} \tag{20}$$

$$Q_{12}^0 = Q_{21}^0 = Q_{12}^{90} = Q_{21}^{90} = \frac{\nu_{12}^y E_2^y}{1 - \nu_{12}^y \nu_{21}^y} \tag{21}$$

$$Q_{22}^0 = Q_{11}^{90} = \frac{E_2^y}{1 - \nu_{12}^y \nu_{21}^y} \tag{22}$$

$$Q_{66}^0 = Q_{66}^{90} = G_{12}^y \tag{23}$$

and $Q_{ij}^0 = Q_{ij}^{90} = 0$ when either $i = 6$ or $j = 6$. A and D become

$$[A] = \begin{bmatrix} A_{11} & A_{12} & 0 \\ A_{12} & A_{11} & 0 \\ 0 & 0 & A_{66} \end{bmatrix} \tag{24}$$

$$[D] = \begin{bmatrix} D_{11} & D_{12} & 0 \\ D_{12} & D_{11} & 0 \\ 0 & 0 & D_{66} \end{bmatrix} \tag{25}$$

Because extension-flexure coupling B_{ij} is zero, apparent in-plane and flexure moduli of the lamina are obtained by the inversion of A and D matrices as follows:

$$2h[A]^{-1} = \begin{bmatrix} \frac{1}{\bar{E}_1} & -\frac{\bar{\nu}_{21}}{\bar{E}_2} & \frac{\bar{\eta}_{12}}{\bar{G}_{12}} \\ -\frac{\bar{\nu}_{12}}{\bar{E}_1} & \frac{1}{\bar{E}_2} & \frac{\bar{\mu}_{12}}{\bar{G}_{12}} \\ \frac{\bar{\eta}_1}{\bar{E}_1} & \frac{\bar{\mu}_2}{\bar{E}_2} & \frac{1}{\bar{G}_{12}} \end{bmatrix} \tag{26}$$

$$[D]^{-1} = \begin{bmatrix} \frac{1}{\overline{EI}_{11}} & \frac{1}{\overline{EI}_{12}} & \frac{1}{\overline{EI}_{13}} \\ \frac{1}{\overline{EI}_{21}} & \frac{1}{\overline{EI}_{22}} & \frac{1}{\overline{EI}_{23}} \\ \frac{1}{\overline{EI}_{31}} & \frac{1}{\overline{EI}_{32}} & \frac{1}{\overline{EI}_{33}} \end{bmatrix} \tag{27}$$

$$\bar{E}_1 = \bar{E}_2 = \frac{A_{11}^2 - A_{12}^2}{2hA_{11}} \tag{28}$$

$$\bar{\nu}_{12} = \bar{\nu}_{21} = \frac{A_{12}}{A_{11}} \tag{29}$$

$$\bar{G}_{12} = \frac{A_{66}}{2h} = G_{12}^{y} \tag{30}$$

$$\overline{EI}_{11} = \overline{EI}_{22} = D_{11} - \frac{D_{12}^2}{D_{11}} \tag{31}$$

$$\overline{EI}_{12} = \overline{EI}_{21} = \frac{D_{11}^2}{D_{12}} - D_{12} \tag{32}$$

$$\overline{EI}_{33} = D_{66} \tag{33}$$

where $\overline{EI}_{13} = \overline{EI}_{31} = \overline{EI}_{23} = \overline{EI}_{32} = 0$; the coupling coefficients associated with membrane behavior are $\bar{\eta}_{12} = \bar{\mu}_{12} = \bar{\eta}_1 = \bar{\mu}_2 = 0$.

2. Two and Three Plies

Material properties of two- (0,0) and three-ply (0,0,0) woven laminates are then obtained by adding more 0 and 90 deg subcells through the thickness of the unit cell as discussed in the preceding subsection. During lay-up process, the fibers in a ply may be in-phase or out-of-phase, or staggered with respect to the fibers in the next ply as discussed in the following section. However, the stiffnesses of these configurations obtained using CLT are all the same:

$$A_{ij} = nh(Q_{ij}^0 + Q_{ij}^{90}) \tag{34}$$

$$B_{ij} = 0 \tag{35}$$

$$D_{ij} = n^3 \frac{h^3}{3}(Q_{ij}^0 + Q_{ij}^{90}) \tag{36}$$

where n is the number of plies. The in-plane elastic constants $\bar{E}_1$, $\bar{E}_2$, $\bar{\nu}_{12}$, $\bar{\nu}_{12}$, and $\bar{G}_{12}$ are equal to the elastic constants of single-ply whereas the flexure moduli of the laminate $\overline{EI}_{11}$, $\overline{EI}_{22}$, $\overline{EI}_{12}$, $\overline{EI}_{21}$, and $\overline{EI}_{33}$ are multiplied by n^3.

B. Finite Element Model

Higher fidelity models are developed to predict the bending properties of plain-weave T300/LTM45 composite. One-, two-, and three-ply woven laminates are modeled using the FE program Abaqus [9]. Based on the unit cell, initially curved beams are used to model each infiltrated fiber yarn. The curved shape of the beam is taken to be a sine curve, $y = h\sin(2\pi x/L)$. The cross section of each beam is approximated by a rectangle of area, 1.375×0.055 mm, equal to that of the infiltrated yarn observed in micrographs of the laminate cross section. The material properties of the beam are taken to be same as the homogenized properties of the infiltrated yarn.

Figure 6 shows a plain-weave lamina with 6×15 units (i.e., 7 yarns in warp and 16 yarns in weft direction). The interlaced yarns are

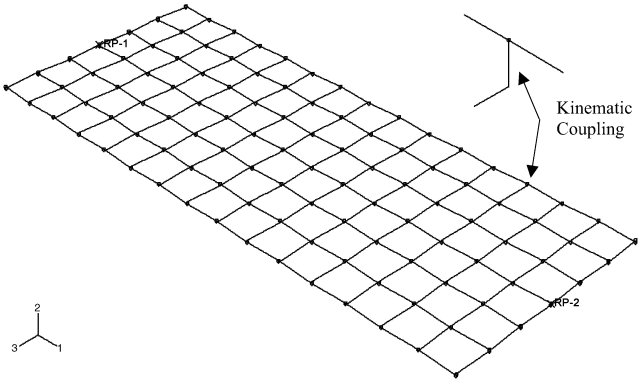

Fig. 6 Plain-weave lamina model (single-ply: 6 × 15 units).

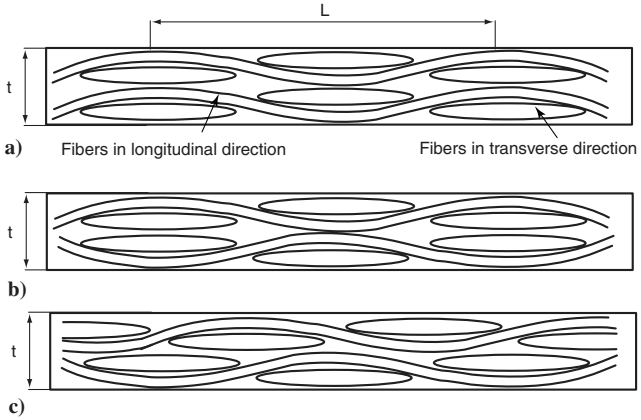

Fig. 7 Schematic cross section of two-ply laminates: a) fibers in phase, b) fibers out of phase, and c) fibers staggered.

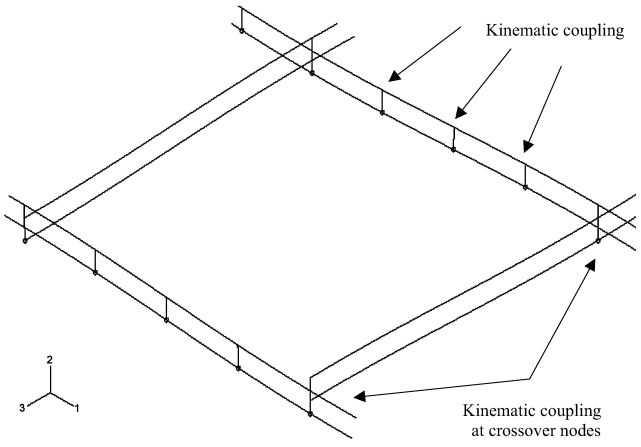

Fig. 8 Plain-weave laminate model (two plies).

constrained at the crossover points kinematically, representing the bonding between the yarns, and transferring loads from one yarn to another. Kinematic constraints are imposed at the coupling nodes of the crossover points. Three rotational degrees of freedom along with three displacement degrees of freedom are constrained by eliminating the specified degrees of freedom at the coupling nodes, which is equivalent to multipoint constraint (MPC) type beam in Abaqus.

The ends of the model are constrained to be rigid using MPC-type tie for the crossover nodes at the ends, that are connected to a reference point placed in the midplane of the structure at either end. MPC-type tie makes the global displacements and rotations as well as all other active degrees of freedom equal at two nodes. The model

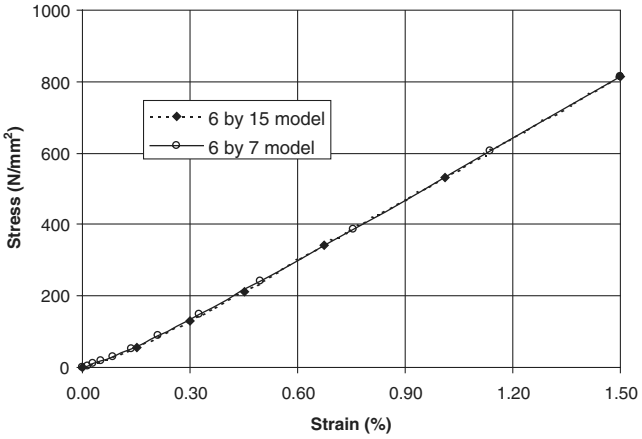

Fig. 9 Stretching simulation of one-ply models.

is meshed using two-node cubic beam elements B33. A geometrically nonlinear analysis of the resulting "space frame" is carried out.

To verify the FE model, first stretching simulation is carried out because in-plane properties are expected to be accurate. For stretching simulation, one end of the model is assumed to be fixed whereas the other end of the model is subjected to prescribed displacement via corresponding reference point. Then for bending simulation prescribed rotations (which are equal and opposite) are applied at both ends via the reference points, and geometrically nonlinear analyses are carried out. The simulations of one-, two-, and three-ply models are studied, and discussed in what follows.

For a two-ply laminate $[0]_2$, the alignment of the warp or weft fibers plays a significant role on bending properties of the material. Three cases are considered: 1) the warp and the weft fibers are in phase, i.e., parallel to each other; 2) the warp and the weft fibers are out of phase, i.e., opposite direction of each other; and 3) the warp and the weft fibers are staggered as in Fig. 7. Figure 8 shows a two-ply laminate (0,0) model, where the warp or the weft fibers are running in parallel to each other as in Fig. 7a. Top and bottom layers are constrained again at the crossover points using kinematic coupling. Preliminary results showed that the longitudinal fibers suffered localized deformations when subject to high curvatures, yielding nonlinear behavior for the bending stiffness as well as the bending strains. This is due to fact that the matrix holds the fibers in place so that there is no significant relative motion of the fibers through the thickness in a cross section. The model was then modified with minimal changes: three more nodes, which are equally spaced between two consecutive crossover points of the same warp yarn, were coupled with their counterparts, connecting top and bottom layers.

IV. Results and Discussion

A. Stretching Simulation

To see the effect of model size on the material properties, two different FE models, 6×7 units (9.625 mm wide and 9.625 mm long) and 6×15 units (9.625 mm wide and 20.625 mm long) are considered. The results of nonlinear analysis are compared in Fig. 9, in which the stress and the strain values are obtained considering the reactions at the reference points of the model and the global dimensions of the model. The longitudinal yarns are subject to uniform high strains whereas the strains of transverse yarns are negligible. The longitudinal yarns are under combined effect of bending and stretching due to the crimp. According to simulations there is an initial nonlinearity due to the crimp of the fibers, and increased model size does not play a significant role on the stiffness. Ignoring the initial nonlinearity, the elastic modules and Poisson's ratios of the one-ply composite are compared in Table 2. As expected the longitudinal stiffness is captured very well with only 1% difference from the manufacturer's data. Note that the model size

Table 2 Comparison of in-plane properties of one ply

	$E_1 = E_2$, GPa	$\nu_{12} = \nu_{21}$
6×7 model	55.6	0.08
6×15 model	55.5	0.04
Manufacturer's data	56.0	——
Rule of mixtures [Eqs. (7) and (8)]	59.0	0.26
CLT [Eqs. (28) and (29)]	61.9	0.03

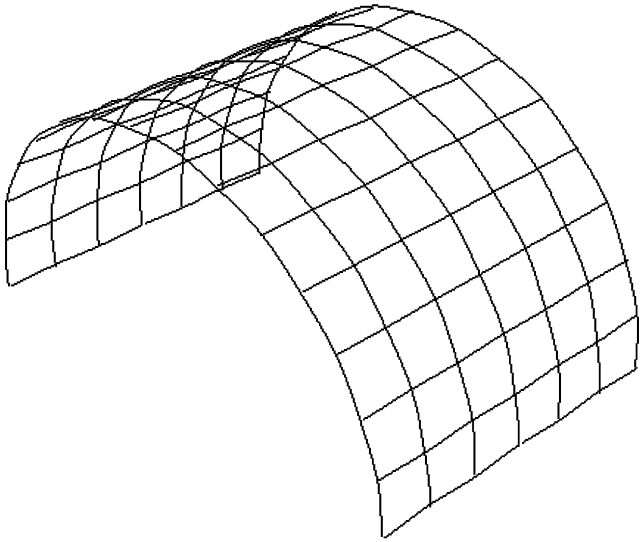

Fig. 10 Single-ply model (6 × 15 units) bent 180 deg.

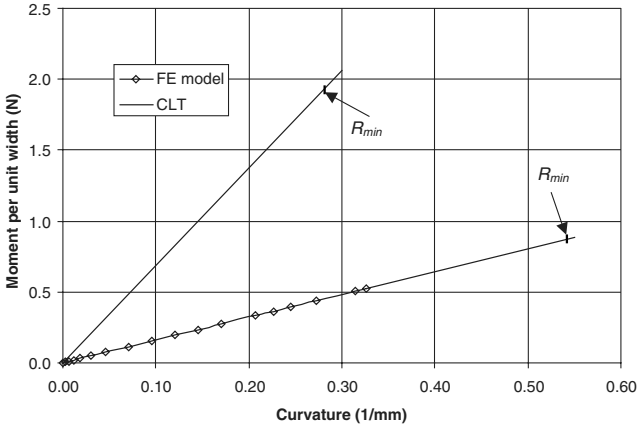

Fig. 11 Moment per unit width vs curvature (single ply, 6 × 7 units).

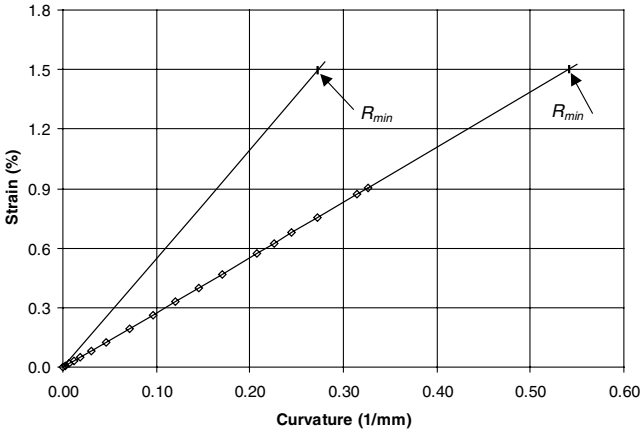

Fig. 12 Strain vs curvature (single ply, 6 × 7 units).

Table 3 Bending stiffness and minimum radius of curvature of one ply

Single ply	D_{11}, Nmm	R_{min}, mm
6×7 model	1.61	1.85
6×15 model	1.61	1.84
Experiment [10]	1.54–1.57	1.69–1.85
CLT [Eqs. (36) and (16)]	6.86	3.67

affects the Poisson's ratio; however, this is not of current interest. The rule of mixtures overestimates both the elastic modulus and the Poisson's ratio. CLT yields $G_{12} = 2.5$ GPa, and still overestimates the elastic modulus because the crimp angle is not taken into account, but the Poisson's ratio is in agreement with the result of simulations.

B. Bending Simulation

1. Single Ply

Single-ply FE models consist of 6×7 units and 6×15 units. Figure 10 shows a one-ply model (6×15 units) which is 180 deg bent. According to the simulation the warp fibers are subject to high strains and stresses whereas the strains and stresses of the weft fibers are not significant. The extreme strains and stresses occur at the outer fiber of the beams representing the warp fibers. The variation of longitudinal strains and stresses along the warp yarns is almost uniform.

Figures 11 and 12 show the bending moment per unit width vs the curvature and the maximum strain vs the curvature obtained from both the FE model (6×7 units) and CLT, respectively. Linear bending behavior of the model is observed. The bending stiffness and the minimum-bending radius of the models are compared with the experimental data [10] as well as to those of CLT in Table 3. The minimum-bending radii of the models correspond to the maximum strain of 1.5%, which is the ultimate strain of the fiber. Both models (6×7 and 6×15) yield similar results, which are in good agreement with the experimental values. Note that the experimental data give a range for different specimen size. When compared with the average experimental data, there is only 3% difference in the bending stiffness, and 4% difference in the minimum bend radius. Clearly CLT overestimates both the bending stiffness and the minimum bend radius by a factor of 4.4 and 2, respectively.

2. Two Plies

Bending simulations are carried out for three cases: 1) fibers in phase, 2) fibers out of phase, and 3) fibers staggered, the results of which are discussed in what follows. To compare results to the experimental data, the thickness of each yarn and the total thickness of the model are taken to be 0.05 and 0.2 mm, respectively.

Results of case 1 are given in Figs. 13 and 14 for moment per unit width versus curvature and strain versus curvature for both the FE model (6×15 units) and CLT, respectively. Again linear bending behavior of the model is observed. Figure 15 shows the model bent

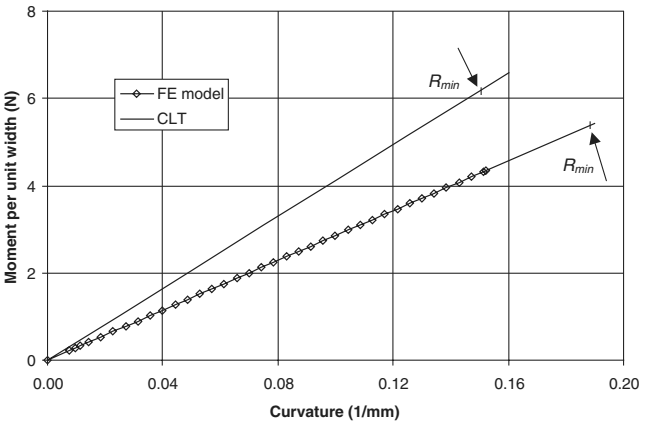

Fig. 13 Moment per unit width vs curvature (two plies, 6 × 15 units).

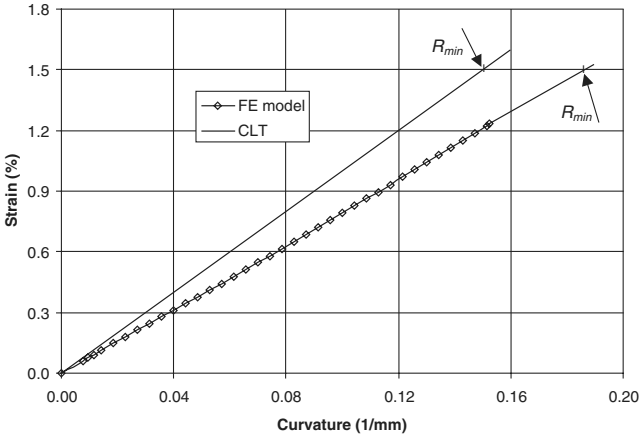

Fig. 14 Strain vs curvature (two plies, 6 × 15 units).

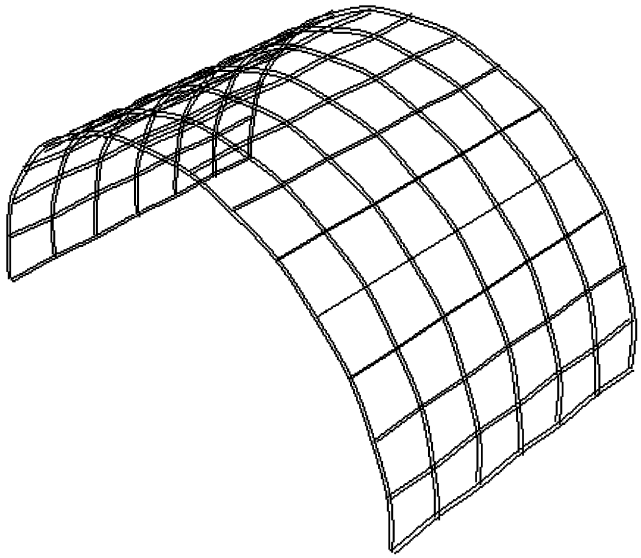

Fig. 15 Two-ply model bent 180 deg (fibers in phase, 6 × 15 units).

180 deg. When the fibers are in phase, the distance between longitudinal fibers is constant, and hence the model bends like a homogenous plate: the outer fibers in a cross section are subject to high strains (tension at the top and compression at the bottom), and the variation of longitudinal strains along the warp fibers is uniform. The bending stiffness and the minimum-bending radius of the

Table 4 Bending stiffness and minimum radius of curvature of two plies

Single ply	D_{11}, Nmm	R_{min}, mm
6×15 model (fibers in phase)	28.51	5.38
6×7 model (fibers in phase)	28.11	5.49
6×7 model (fibers out of phase)	17.08	6.87
6×7 model (fibers staggered)	18.60	6.50
Experiment [10]	18.3–22.7	4.76–5.26
CLT [Eqs. (36) and (16)]	41.24	6.67

Table 5 Bending stiffness and minimum radius of curvature of three plies

Single ply	D_{11}, Nmm	R_{min}, mm
6×7 model (fibers in phase)	144.12	10.18
CLT [Eqs. (36) and (16)]	185.27	11.00

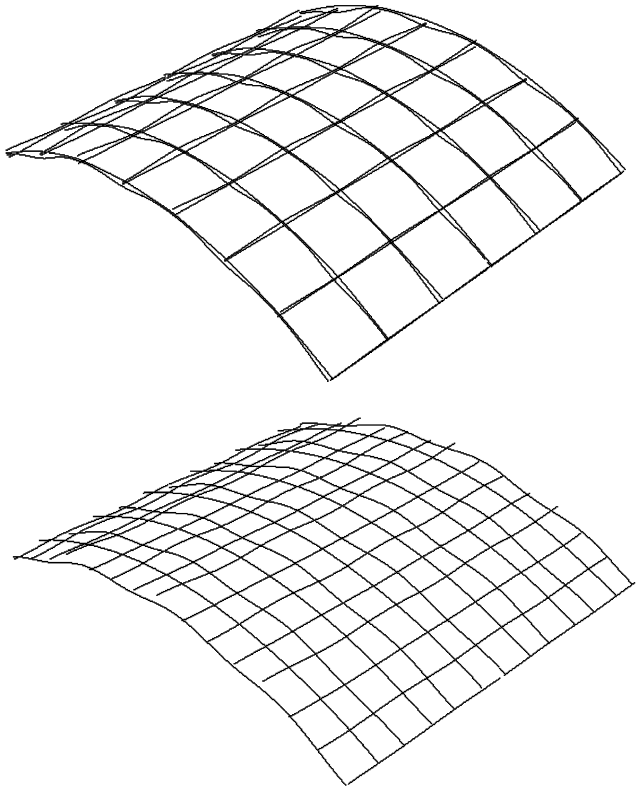

Fig. 16 Two-ply models (6 × 7 units); fibers out of phase (top) and staggered (bottom).

models are compared with experimental data [10] as well as to those of CLT in Table 4. The experimental data give a range for different specimen size again. When compared with the average experimental data, CLT overestimates both the bending stiffness and the minimum bend radius by 101% and 33%, respectively, but this time the FE model (6 × 15 units) overestimates both the bending stiffness and the minimum bend radius by 39% and 7%, respectively.

Case 2, in which the fibers of one ply are out of phase with respect to the fibers of the other ply as in Fig. 7b, is also studied, the results of which are given in Table 4. When compared with the experimental data, the model with 6 × 7 units yields less bending stiffness by 13% whereas it overestimates the minimum bend radius by 37%. When the fibers are out of phase, the distance between longitudinal fibers is not constant. Figure 16 (top) shows the model bent 60 deg: high strains appear at every other crossover point where the distance between upper and lower longitudinal yarns is minimum.

In case 3, the fibers are staggered as in Fig. 7c; the distance between longitudinal fibers is not constant. Because the minimum distance of the longitudinal fibers is less than that of case 1 and greater than that of case 2, it yields that the bending stiffness and the bending radius are between those of case 1 and case 2 as given in Table 4. The results are based on linear analysis due to the fact that nonlinear analysis of the model yields convergence problems. The model bent 54 deg is given Fig. 16 (bottom). The models of the case 1 and case 2 yield upper and lower bounds for the bending stiffness. The experimental data, which are within the bounds, are based on the specimens manufactured by not considering fiber alignment in microlevel. Alignment of the fibers in microlevel is not practical.

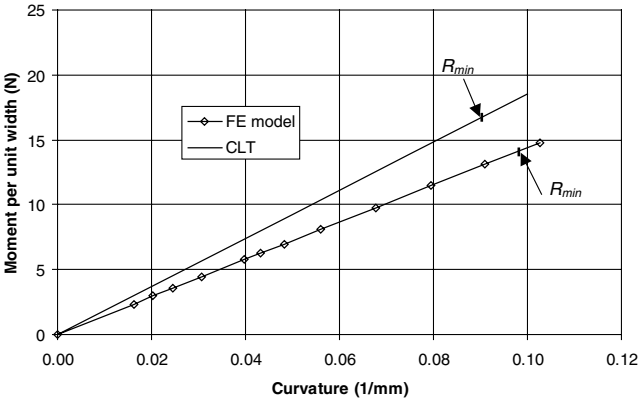

Fig. 17 Moment per unit width vs curvature (three plies, 6 × 7 units).

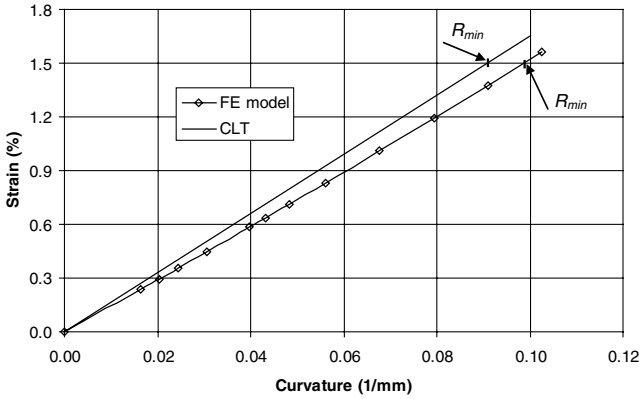

Fig. 18 Strain vs curvature (three plies, 6 × 7 units).

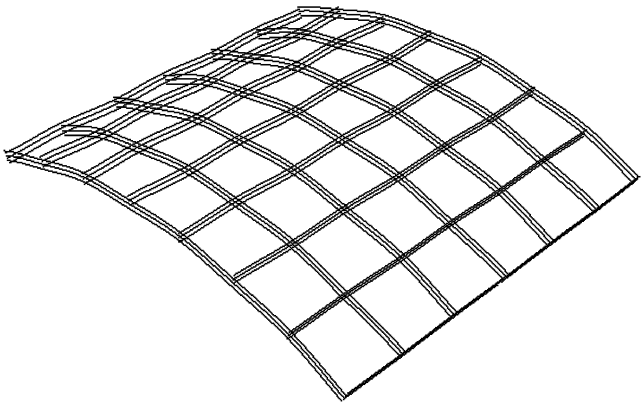

Fig. 19 Three-ply model bent 50 deg (fibers are in phase, 6 × 7 units).

3. Three Plies

A three-ply FE model with 6 × 7 units, in which the fibers in a ply are in phase with the fibers of the other plies as in Fig. 7a, is considered. Nominal values for the thickness of each yarn and the total thickness of the model are taken to be 0.055 and 0.33 mm, respectively. Figures 17 and 18 show the bending moment per unit width versus curvature and the maximum strain versus curvature for both the FE model (6 × 7 units) and CLT, respectively. Linear bending behavior is observed again. When compared with the FE model, CLT still overestimates the bending stiffness by 28.6% and the minimum-bending radius by 8%; see Table 5. Figure 19 shows the model bent 50 deg, in which the outer fibers in a cross section are subject to high strains (tension at the top and compression at the bottom), and the variation of longitudinal strains along the warp fibers is uniform.

V. Conclusions

Micromechanical models have been developed to predict bending properties of plain-weave composites. Behavior of one-, two-, and three-ply laminates is investigated by the mosaic model using the classical plate theory as well as higher fidelity finite element models.

Although in-plane properties of the laminates are predicted well using both the mosaic and finite element models, predictions for the bending behavior of the laminates based on the classical plate theory disagree with the experimental results [10]. The results of single-ply models based on finite element analysis are in good agreement with the experimental data. For a two-ply laminate, the alignment of the fibers plays significant role in bending behavior. Three cases are considered: 1) fibers in phase, 2) fibers out of phase, and 3) fibers staggered. The results of the first two cases yield upper and lower bounds for the bending stiffness; the experimental data (within the bounds and close to the bending stiffness of case 3) are based on the specimens manufactured by not considering the fiber alignment in microlevel. The predictions based on CLT for a three-ply laminate approach the values obtained by finite element models.

Acknowledgment

Discussions with Sergio Pellegrino are gratefully acknowledged.

References

[1] Naik, R. A., "Analysis of Woven and Braided Fabric Reinforced Composites," NASA CR 194930, 1994.

[2] Johnson, E. R., Chretien, N., and Rastogi, N., "Homogenization of a Plain Weave Textile Composite," AIAA Paper 2002-1615, April 2002.

[3] Fujita, A, Hamada, H., and Maekawa, Z., "Tensile Properties of Carbon Fiber Triaxial Woven Fabric Composites," *Journal of Composite Materials*, Vol. 27, No. 15, 1993, pp. 1428–1442.

[4] Dano, M. L., Gendron, G., and Picard, A., "Mechanical Behavior of a Triaxial Woven Fabric Composite," *Mechanics of Composite Materials and Structures*, Vol. 7, No. 2, 2000, pp. 207–224.

[5] Bednarcyk, B. A., and Arnold, S. M., "Micromechanics-Based Modeling of Woven Polymer Matrix Composites," *AIAA Journal*, Vol. 41, No. 9, 2003, pp. 1788–1796.

[6] Le Page, B. H., Guild, F. J., Ogin, S. L., and Smith, P. A, "Finite Element Simulation of Woven Fabric Composites," *Composites, Part A: Applied Science and Manufacturing*, Vol. 35, Nos. 7–8, 2004, pp. 861–872.

[7] Yee, J. C. H., and Pellegrino, S., "Folding of Woven Composite Structures," *Composites, Part A: Applied Science and Manufacturing*, Vol. 36, No. 2, 2005, pp. 273–278.

[8] Daniel, I. M., and Ishai, O., *Engineering Mechanics of Composite Materials*, Oxford Univ. Press, Oxford, 1994.

[9] Hibbit, K., ABAQUS/Standard User's Manual, Ver. 6.4., Sorensen, Inc., Pawtucket, RI, 2004.

[10] Yee, J. C. H., and Pellegrino, S., "Biaxial Bending Failure Locus for Woven-Thin-Ply Carbon Fibre Reinforced Plastic Structures," AIAA Paper 2005-1811, April 2005.

G. Agnes
Associate Editor